Engineering Fracture Mechanics 132 (2014) 177–188

Contents lists available at ScienceDirect

Engineering Fracture Mechanics

journal homepage: www.elsevier.com/locate/engfracmech

Stress fields induced by a non-uniform displacement discontinuity in an elastic half plane

Amirhossein Molavi Tabrizi [a], Ernie Pan [a,*], Stephen J. Martel [b], Kaiming Xia [c], W. Ashley Griffith [d], Ali Sangghaleh [a]

[a] Department of Civil Engineering, University of Akron, Akron, OH 44325, USA
[b] Department of Geology and Geophysics, University of Hawaii, Honolulu, HI 96822, USA
[c] Shell International Exploration and Production Inc., Westhollow Technology Center, Houston, TX 77001, USA
[d] Department of Earth and Environmental Sciences, University of Texas at Arlington, Arlington, TX 76019, USA

ARTICLE INFO

Article history:
Received 31 March 2014
Received in revised form 25 September 2014
Accepted 7 October 2014
Available online 14 October 2014

Keywords:
Green's function
Displacement discontinuity
Non-uniform
Complex potential function
Fault
Hydraulic fracturing

ABSTRACT

This paper presents the exact closed-form solutions for the stress fields induced by a two-dimensional (2D) non-uniform displacement discontinuity (DD) of finite length in an isotropic elastic half plane. The relative displacement across the DD varies quadratically. We employ the complex potential-function method to first determine the Green's stress fields induced by a concentrated force and then apply Betti's reciprocal theorem to obtain the Green's displacement fields due to concentrated DD. By taking the derivative of the Green's functions and integrating along the DD, we derive the exact closed-form solutions of the stress fields for a quadratic DD. The solutions are applied to analyze the stress fields near a horizontal DD in the half plane with three different profiles: uniform (constant), linear, and quadratic. The same methodology is applied to an inclined normal fault to investigate the effect of different DD profiles on the maximum shear stress in the half plane as well as on the normal and shear stresses along the fault. Numerical results demonstrate considerable influence of the DD profile on the stress distribution around the discontinuity.

1. Introduction

Scientists and engineers study cracks for many reasons. Two key reasons are to (1) understand the associated stress concentrations or singularity features, and (2) accurately predict the life span of cracked structures or media.

Numerical methods such as the finite element method (FEM) and boundary element method (BEM) have been utilized by many researchers to solve crack problems. The BEM based on displacement discontinuity (DD) has been proved to be particularly efficient [1–3]. The indirect BEM also has been used to treat single and multiple displacement discontinuities (DDs) in 2D finite and infinite regions [4] and to calculate stress intensity factors at crack tips in 2D anisotropic elastic solids [5]. An accurate single-domain BEM for 2D infinite, finite, and semi-infinite anisotropic solids [6] has been extended to three-dimensional (3D) anisotropic media [7]. The Riemann–Hilbert method can be adopted to solve 2D crack problems in an infinite, homogeneous, anisotropic plate [8]. A general higher-order DD method coupled with an indirect BEM has been applied to the quasi-static analyses of radial cracks produced by blasting [9]. Complex crack problems such as multiple branched and intersecting cracks also have been investigated using the numerical manifold method [10], which also has been applied to 2D

* Corresponding author. Tel.: +1 330 972 6739; fax: +1 330 972 6020.
E-mail address: pan2@uakron.edu (E. Pan).

http://dx.doi.org/10.1016/j.engfracmech.2014.10.009
0013-7944/

Nomenclature

Latin

a_j, b_j, c_j	constants to determine the relative displacement discontinuity profile in j-direction
A, B	complex constants
$f_1()$, $f_2()$, $f_3()$	function of
F_x, F_y	line force component along x- and y-direction respectively
i	imaginary unit
k_1, k_2, …, k_{15}	complex variables
L	length of displacement discontinuity
$\boldsymbol{n}$	normal vector
n_p	p-component of normal vector
p, q, r, s, w	dummy complex variables
t	parameter that varies between 0 and 1 along the displacement discontinuity
t_m	location along displacement discontinuity between 0 and 1 at which relative displacement is known; $0 < t_m < 1$
u_k	displacement component in k-direction
$u_{k,j}$	derivative of k-component of displacement with respect to coordinate j
$\Delta\boldsymbol{u}$	relative displacement discontinuity vector
Δu_{j1}, Δu_{j2}	relative displacement discontinuities along j-direction at starting and ending points of displacement discontinuity
Δu_{jm}	relative displacement discontinuities along j-direction at $t = t_m$
Δu_q	relative displacement discontinuities along q-direction
x, y	coordinates of the field point of the line force
x_1, x_2; y_1, y_2	coordinates of starting and ending points of displacement discontinuity
x_s, y_s	coordinates of the source point of the line force
z, z_s	complex variable to define a field point and source point of the line force
z_1, z_2	complex variables to define starting and ending points of displacement discontinuity

Greek

α_j, β_j, γ_j	constants related to the profile of displacement discontinuity
Γ_1, Γ_2	complex functions
Γ_{1p}, Γ_{2p}	complex functions corresponding to particular solution
Γ_{1c}, Γ_{2c}	complex functions corresponding to complementary solution
ε_{xx}, ε_{yy}, γ_{xy}	strain components
μ	shear modulus
ν	Poisson's ratio
σ^k_{pq}	pq component of stress induced by a line force in k-direction
$\sigma^k_{pq,j}$	derivative of pq-component of stress induced by a line force in k-direction with respect to coordinate j
σ_{xx}, σ_{yy}, σ_{xy}	stress components
$\phi()$, $\psi()$	complex functions
$\phi_p()$, $\psi_p()$	complex functions which describe the particular solution in an infinite plane
$\phi_c()$, $\psi_c()$	complex functions which describe the complementary solution of the half plane
Ω_1, Ω_2	complex functions
Ω_{1p}, Ω_{2p}	complex functions corresponding to particular solution
Ω_{1c}, Ω_{2c}	complex functions corresponding to complementary solution

Acronyms

2D	two-dimensional
3D	three-dimensional
BEM	boundary element method
DD	displacement discontinuity
FEM	finite element method

crack propagation [11]. Moreover, the growth of short fatigue cracks has been studied by 2D DD BEM [12]. Axisymmetric crack problems have been analyzed with the axisymmetric DD method [13].

DD-based BEM analyses have been applied to a variety of problems in geology, especially those involving faults. These models have been used to simulate the behavior and interaction of intersecting faults in both 2D and 3D [14,15], and the

development of secondary fractures near faults [16]. These models also have been used to study mixed-mode fracture propagation in an isotropic 3D medium [17], elastic stresses in long ridges [18], and stresses associated with the initial stages of landsliding [19,20]. DD-based BEM can also be used to investigate the role of static friction on fracture orientation along strike-slip faults [21]. These investigations confirm that the DD method is flexible and particularly attractive in solving geological problems.

Motivated by the important applications of the DD method in the earth sciences as well as in the oil and gas industries where faults and hydraulic fractures are important, we present here the exact closed-form solution for a non-uniform DD in an isotropic elastic half plane. In Section 2, the problem is described and the exact closed-form solution is derived. Using numerical examples, the stress fields arising from three DD profiles (uniform, linear, and quadratic) are presented and compared in Section 3. The key conclusions are summarized in Section 4.

2. Solution to a non-uniform displacement discontinuity in a half plane

We consider first a DD vector $\Delta\boldsymbol{u}$ at a point $z = x + iy$ in the complex isotropic elastic half plane with the DD line plane normal being $\boldsymbol{n}$. The induced displacement u_k in the k-direction at $z_s = x_s + iy_s$ can be expressed using a relationship based on Betti's reciprocal theorem [22].

$$u_k(z_s) = \int_L \sigma^k_{pq}(z_s; z)\Delta u_q(z) n_p(z) dL(z) \tag{1}$$

where the summation convention is implied for repeated indices p and q. In other words, they both take summations from 1 to 2 (i.e., from x to y). Also in Eq. (1), L is the length of DD, and $\sigma^k_{pq}(z_s; z)$ is the stress with component pq at z induced by a line force (per unit length) in k-direction applied at z_s; $\sigma^k_{pq}(z_s; z)$ thus has dimensions of 1/length.

In order to find the DD-induced stress field, one needs to take the derivative of Eq. (1) with respect to the line-force location z_s.

$$u_{k,j}(z_s) = \int_L \sigma^k_{pq,j}(z_s; z)\Delta u_q(z) n_p(z) dL(z) \tag{2}$$

where the derivative for index j is with respect to x_s or y_s.

The constitutive relation in 2D plane-strain deformation can be applied to find the stresses as follows:

$$\begin{bmatrix} \sigma_{xx} \\ \sigma_{yy} \\ \sigma_{xy} \end{bmatrix} = \frac{2\mu}{(1-2\nu)} \begin{bmatrix} 1-\nu & \nu & 0 \\ \nu & 1-\nu & 0 \\ 0 & 0 & (1-2\nu)/2 \end{bmatrix} \begin{bmatrix} \varepsilon_{xx} \\ \varepsilon_{yy} \\ \gamma_{xy} \end{bmatrix} \tag{3}$$

where μ and ν are the shear modulus and Poisson's ratio, respectively [23].

In order to find the DD $\Delta\boldsymbol{u}$-induced displacement, strain, and stress fields, one first needs to find the line-force-induced stress field σ^k_{pq} as it appears in Eq. (1). We adopt the complex variable function method of Muskhelishvili [24] to derive the solution. We assume a concentrated line force $(F_x + iF_y)$ located at $z_s = x_s + iy_s$ in an isotropic elastic and homogeneous half plane $y > 0$. The surface of the half plane is assumed to be traction-free. From Muskhelishvili [24], the plane stresses can be expressed in terms of two complex functions ϕ and ψ of the complex variable $z = x + iy$.

$$\begin{aligned} &\sigma_{xx} + \sigma_{yy} = 2[\phi'(z) + \overline{\phi'(z)}] \\ &\sigma_{yy} - \sigma_{xx} + 2i\sigma_{xy} = 2[\bar{z}\phi''(z) + \psi'(z)] \end{aligned} \tag{4}$$

where the overbar denotes the conjugate of a complex variable or function, and the prime indicates the derivative of the function with respect to z. For the half plane case, these complex functions can be separated into two parts: a particular solution with subscript "p" for the infinite plane, and a complementary part with subscript "c" that is introduced to satisfy the traction-free boundary condition on the surface of the half plane.

$$\begin{aligned} &\phi(z) = \phi_p(z) + \phi_c(z) \\ &\psi(z) = \psi_p(z) + \psi_c(z) \end{aligned} \tag{5}$$

For a line force located at z_s, these complex functions are

$$\phi_p(z) = A\ln(z - z_s), \quad \psi_p(z) = B\ln(z - z_s) - A\frac{\bar{z}_s}{z - z_s} \tag{6a}$$

$$\begin{aligned} &\phi_c(z) = -\left[\overline{A}\tfrac{z-z_s}{z-\bar{z}_s} + \overline{B}\ln(z - \bar{z}_s)\right] \\ &\psi_c(z) = -\overline{A}\ln(z - \bar{z}_s) + z\left[\tfrac{\overline{A}+\overline{B}}{z-\bar{z}_s} - \overline{A}\tfrac{z-z_s}{(z-\bar{z}_s)^2}\right] \end{aligned} \tag{6b}$$

where again $z = x + iy$ is the field point in the complex plane and A and B are two complex constants:

$$A=\frac{-(F_x+iF_y)}{8\pi(1-\nu)};\quad B=\frac{(3-4\nu)(F_x-iF_y)}{8\pi(1-\nu)} \tag{7}$$

Substituting Eqs. (6) into Eq. (4), the stress field induced by the concentrated line force at z_s can be obtained.

$$\begin{aligned}\Omega_1&\equiv[\sigma_{xx}+\sigma_{yy}]/2=\Omega_{1p}+\Omega_{1c}\\ \Omega_2&\equiv[\sigma_{yy}-\sigma_{xx}+2i\sigma_{xy}]/2=\Omega_{2p}+\Omega_{2c}\end{aligned} \tag{8}$$

with the particular part being the solution for the full plane. The particular and complementary parts of the stress fields due to the concentrated line force in the half plane can be expressed as follows:

$$\begin{aligned}\Omega_{1p}&\equiv[\sigma_{xx}+\sigma_{yy}]_p/2=\tfrac{A}{z-z_s}+\tfrac{\bar{A}}{\bar{z}-\bar{z}_s}\\ \Omega_{2p}&\equiv[\sigma_{yy}-\sigma_{xx}+2i\sigma_{xy}]_p/2=\tfrac{B}{z-z_s}+\tfrac{A(\bar{z}_s-\bar{z})}{(z-z_s)^2}\end{aligned} \tag{9}$$

$$\begin{aligned}\Omega_{1c}&\equiv[\sigma_{xx}+\sigma_{yy}]_c/2=-\tfrac{\bar{A}+\bar{B}}{z-\bar{z}_s}-\tfrac{A+B}{\bar{z}-z_s}+\tfrac{\bar{A}(z-z_s)}{(z-\bar{z}_s)^2}+\tfrac{A(\bar{z}-\bar{z}_s)}{(\bar{z}-z_s)^2}\\ \Omega_{2c}&\equiv[\sigma_{yy}-\sigma_{xx}+2i\sigma_{xy}]_c/2=\tfrac{\bar{B}}{(\bar{z}-z_s)}-\tfrac{\bar{A}(z-z_s)}{(z-\bar{z}_s)^2}+(z-\bar{z})\left[-\tfrac{2\bar{A}+\bar{B}}{(z-\bar{z}_s)^2}+\tfrac{2\bar{A}(z-z_s)}{(z-\bar{z}_s)^3}\right]\end{aligned} \tag{10}$$

We point out that with the line-force induced stresses in Eqs. (9) and (10), one can find the DD-induced displacement field via Eq. (1). In order to find the DD-induced stress field, the derivatives of the line-force induced stress field with respect to (x_s, y_s) are required which are presented below.

$$\begin{aligned}\frac{\partial\Omega_{1p}}{\partial x_s}&\equiv\frac{\partial\Omega_{1p}}{\partial z_s}+\frac{\partial\Omega_{1p}}{\partial\bar{z}_s}=\frac{A}{(z-z_s)^2}+\frac{\bar{A}}{(\bar{z}-\bar{z}_s)^2}\\ \frac{\partial\Omega_{1p}}{\partial y_s}&\equiv i\left[\frac{\partial\Omega_{1p}}{\partial z_s}-\frac{\partial\Omega_{1p}}{\partial\bar{z}_s}\right]=i\left[\frac{A}{(z-z_s)^2}-\frac{\bar{A}}{(\bar{z}-\bar{z}_s)^2}\right]\end{aligned} \tag{11}$$

$$\begin{aligned}\frac{\partial\Omega_{2p}}{\partial x_s}&\equiv\frac{\partial\Omega_{2p}}{\partial z_s}+\frac{\partial\Omega_{2p}}{\partial\bar{z}_s}=\frac{2A(\bar{z}_s-\bar{z})}{(z-z_s)^3}+\frac{B+A}{(z-z_s)^2}\\ \frac{\partial\Omega_{2p}}{\partial y_s}&\equiv i\left[\frac{\partial\Omega_{2p}}{\partial z_s}-\frac{\partial\Omega_{2p}}{\partial\bar{z}_s}\right]=i\left[\frac{2A(\bar{z}_s-\bar{z})}{(z-z_s)^3}+\frac{B-A}{(z-z_s)^2}\right]\end{aligned} \tag{12}$$

$$\begin{aligned}\frac{\partial\Omega_{1c}}{\partial x_s}&\equiv\frac{\partial\Omega_{1c}}{\partial z_s}+\frac{\partial\Omega_{1c}}{\partial\bar{z}_s}=-\frac{2\bar{A}+\bar{B}}{(z-\bar{z}_s)^2}-\frac{2A+B}{(\bar{z}-z_s)^2}+\frac{2A(\bar{z}-\bar{z}_s)}{(\bar{z}-z_s)^3}+\frac{2\bar{A}(z-z_s)}{(z-\bar{z}_s)^3}\\ \frac{\partial\Omega_{1c}}{\partial y_s}&\equiv i\left[\frac{\partial\Omega_{1c}}{\partial z_s}-\frac{\partial\Omega_{1c}}{\partial\bar{z}_s}\right]=i\left[\frac{\bar{B}}{(z-\bar{z}_s)^2}-\frac{B}{(\bar{z}-z_s)^2}+\frac{2A(\bar{z}-\bar{z}_s)}{(\bar{z}-z_s)^3}-\frac{2\bar{A}(z-z_s)}{(z-\bar{z}_s)^3}\right]\end{aligned} \tag{13}$$

$$\begin{aligned}\frac{\partial\Omega_{2c}}{\partial x_s}&\equiv\frac{\partial\Omega_{2c}}{\partial z_s}+\frac{\partial\Omega_{2c}}{\partial\bar{z}_s}=(z-\bar{z})\left[\frac{6\bar{A}(z-z_s)}{(z-\bar{z}_s)^4}-\frac{2(3\bar{A}+\bar{B})}{(z-\bar{z}_s)^3}\right]-\frac{2\bar{A}(z-z_s)}{(z-\bar{z}_s)^3}+\frac{\bar{A}+\bar{B}}{(z-\bar{z}_s)^2}\\ \frac{\partial\Omega_{2c}}{\partial y_s}&\equiv i\left[\frac{\partial\Omega_{2c}}{\partial z_s}-\frac{\partial\Omega_{2c}}{\partial\bar{z}_s}\right]=i\left[(z-\bar{z})\left[-\frac{6\bar{A}(z-z_s)}{(z-\bar{z}_s)^4}+\frac{2(\bar{A}+\bar{B})}{(z-\bar{z}_s)^3}\right]+\frac{2\bar{A}(z-z_s)}{(z-\bar{z}_s)^3}-\frac{\bar{A}-\bar{B}}{(z-\bar{z}_s)^2}\right]\end{aligned} \tag{14}$$

We assume now a DD distribution of quadratic form along a straight line segment from z_1 to z_2 in the half plane. Our goal is to find the analytical expressions of the stress field induced by this general form of DD in the half plane. To achieve this, we first express the straight line segment in the parametric form.

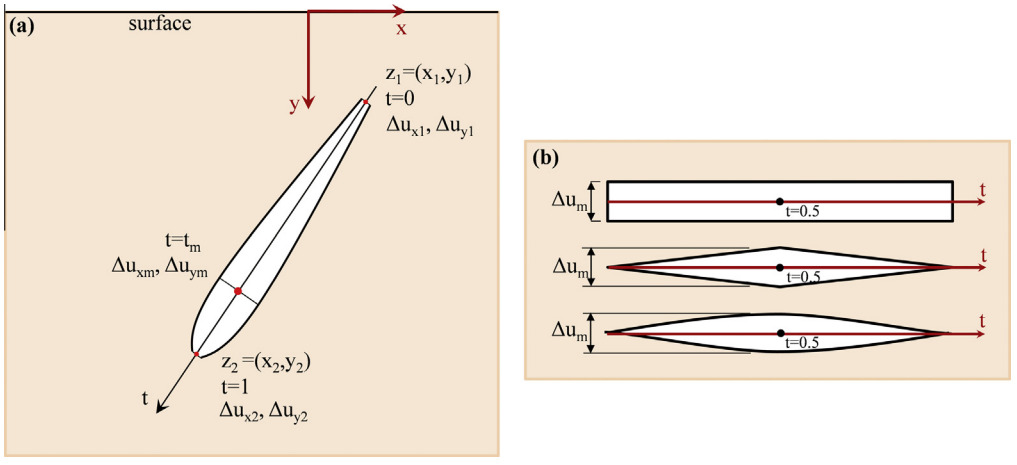

Fig. 1. (a) Schematics of a non-uniform DD in the half plane. (b) Three special cases when the maximum value of Δu occurs in the middle of the DD: a uniform (constant) DD (top), a linear DD (middle), and a parabolic DD (bottom).

$$x = x_1 + (x_2 - x_1)t$$
$$y = y_1 + (y_2 - y_1)t \tag{15}$$

where $t = 0$ and 1 corresponds to $(x,y) = (x_1,y_1)$ and (x_2,y_2), respectively. The length of the DD segment is

$$L = \sqrt{(x_2 - x_1)^2 + (y_2 - y_1)^2} \tag{16}$$

In terms of the parameter t, the quadratic DD Δu_j can be assumed as

$$\Delta u_j = 2(a_j t^2 + b_j t + c_j); \quad j = x, y \tag{17}$$

where a_j, b_j, and c_j are constants which can be determined from values of Δu_j at three arbitrary points along the discontinuity. In this paper, we consider the start and end points of the discontinuity and a point in between, so that

$$a_j = \frac{\Delta u_{jm} - t_m \Delta u_{j2} + t_m \Delta u_{j1} - \Delta u_{j1}}{2t_m(t_m - 1)}$$
$$b_j = \frac{\Delta u_{j2} - \Delta u_{j1}}{2} - \frac{\Delta u_{jm} - t_m \Delta u_{j2} + t_m \Delta u_{j1} - \Delta u_{j1}}{2t_m(t_m - 1)} \quad j = x, y \tag{18}$$
$$c_j = \frac{\Delta u_{j1}}{2}$$

where Δu_{j1}, Δu_{jm}, and Δu_{j2} are the magnitudes of the relative displacement at the start ($t = 0$), at an intermediate point ($t = t_m$), and at the end point ($t = 1$) of the DD line, respectively. Note that t_m varies between 0 and 1, and it does not need to correspond to the point with the maximum value of Δu_j. One special choice is $t_m = 0.5$ which means that the relative displacement Δu_{jm} is at the midpoint. Equation (17) represents a general quadratic DD profile as illustrated in Fig. 1a while Fig. 1b shows three special cases where the maximum DD occurs at $t_m = 0.5$ for the uniform (constant), linear, and quadratic distributions of DD profiles.

Therefore, in terms of parameter t, the DD-induced displacement derivatives can be expressed as follows.

$$\frac{\partial u_k}{\partial x_s} = 2n_p L \int_0^1 \left[\frac{\partial \sigma^k_{pq}}{\partial z_s} + \frac{\partial \sigma^k_{pq}}{\partial \bar{z}_s}\right](a_q t^2 + b_q t + c_q)dt$$
$$\frac{\partial u_k}{\partial y_s} = 2n_p L \int_0^1 \left[i\frac{\partial \sigma^k_{pq}}{\partial z_s} - i\frac{\partial \sigma^k_{pq}}{\partial \bar{z}_s}\right](a_q t^2 + b_q t + c_q)dt \qquad \begin{cases} k = x, y \\ p \text{ or } q = x, y \end{cases} \tag{19}$$

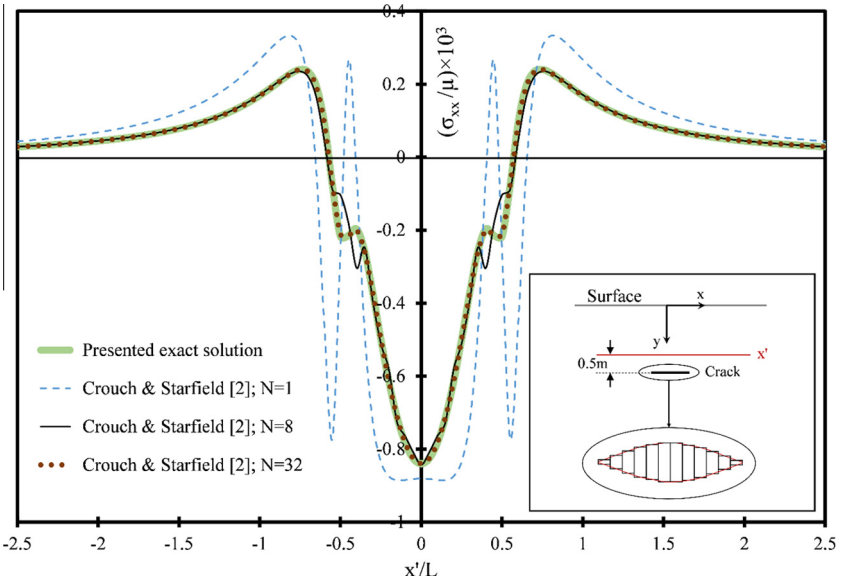

Fig. 2. Normalized horizontal stress σ_{xx}/μ along the horizontal line segment x' (0.5 m above the crack) calculated by the constant DD element solution of Crouch and Starfield [2], as compared to the present exact closed-form solution. The crack opening shape is quadratic and the crack length is 4 m. It is horizontally located at $y = 1000$ m below the surface of the half plane.

Table 1
Maximum relative error for the horizontal stress σ_{xx} calculated by the constant DD element solution of Crouch and Starfield [2], as compared to the present exact closed-form solution of the quadratic DD profile. N represents the number of the discretized constant elements along the crack length.

N	1	2	4	8	16	32	64	128	256	512
Maximum relative error (%)	897.00	647.75	192.68	54.10	12.35	3.01	0.75	0.19	0.05	0.01

Note that for $k = x$, we set $F_x = 1$ and $F_y = 0$ while for $k = y$, $F_x = 0$ and $F_y = 1$. Thus, in terms of the components, the following integrals are needed in order to find the displacement derivatives in Eq. (19).

$$\begin{aligned}\Gamma_{mp,x_s} &= 2L\int_0^1 \frac{\partial\Omega_{mp}}{\partial x_s}(a_jt^2+b_jt+c_j)dt = 2L\int_0^1\left[\frac{\partial\Omega_{mp}}{\partial z_s}+\frac{\partial\Omega_{mp}}{\partial\bar{z}_s}\right](a_jt^2+b_jt+c_j)dt\\ \Gamma_{mp,y_s} &= 2L\int_0^1 \frac{\partial\Omega_{mp}}{\partial y_s}(a_jt^2+b_jt+c_j)dt = 2iL\int_0^1\left[\frac{\partial\Omega_{mp}}{\partial z_s}-\frac{\partial\Omega_{mp}}{\partial\bar{z}_s}\right](a_jt^2+b_jt+c_j)dt\end{aligned} \tag{20}$$

$$\begin{aligned}\Gamma_{mc,x_s} &= 2L\int_0^1 \frac{\partial\Omega_{mc}}{\partial x_s}(a_jt^2+b_jt+c_j)dt = 2L\int_0^1[\frac{\partial\Omega_{mc}}{\partial z_s}+\frac{\partial\Omega_{mc}}{\partial\bar{z}_s}](a_jt^2+b_jt+c_j)dt\\ \Gamma_{mc,y_s} &= 2L\int_0^1 \frac{\partial\Omega_{mc}}{\partial y_s}(a_jt^2+b_jt+c_j)dt = 2iL\int_0^1\left[\frac{\partial\Omega_{mc}}{\partial z_s}-\frac{\partial\Omega_{mc}}{\partial\bar{z}_s}\right](a_jt^2+b_jt+c_j)dt\end{aligned} \tag{21}$$

The exact closed-form expressions for the functions $\Gamma_{mp,xs}$, $\Gamma_{mp,ys}$, $\Gamma_{mc,xs}$, and $\Gamma_{mc,ys}$ are given in the Appendix. Using the constitutive relation in Eq. (3), we can find the corresponding stress field. Note that the particular solution is the full-plane solution and the complementary solution approaches zero far from the surface. As a result, far from the surface the total solution approaches the full-plane solution.

3. Numerical examples

For a straight crack in a linear elastic medium, the relative opening displacements generally are non-uniform. Thus, using a quadratic DD would in many cases yield satisfactory solutions with less discretization and shorter computer runtimes. To investigate the utility of the quadratic DD, we apply our exact closed-form solutions to three DD cases in an isotropic elastic half plane.

In the first numerical example, we calculate the normal stress field σ_{xx} induced by a quadratic DD. Similar to the work by Maerten et al. [25] and Crouch and Starfield [2], in order to approximate the quadratic DD profile, certain numbers of constant DD elements are needed. The results illustrated in Fig. 2 consider a horizontal opening-mode DD of length 4 m

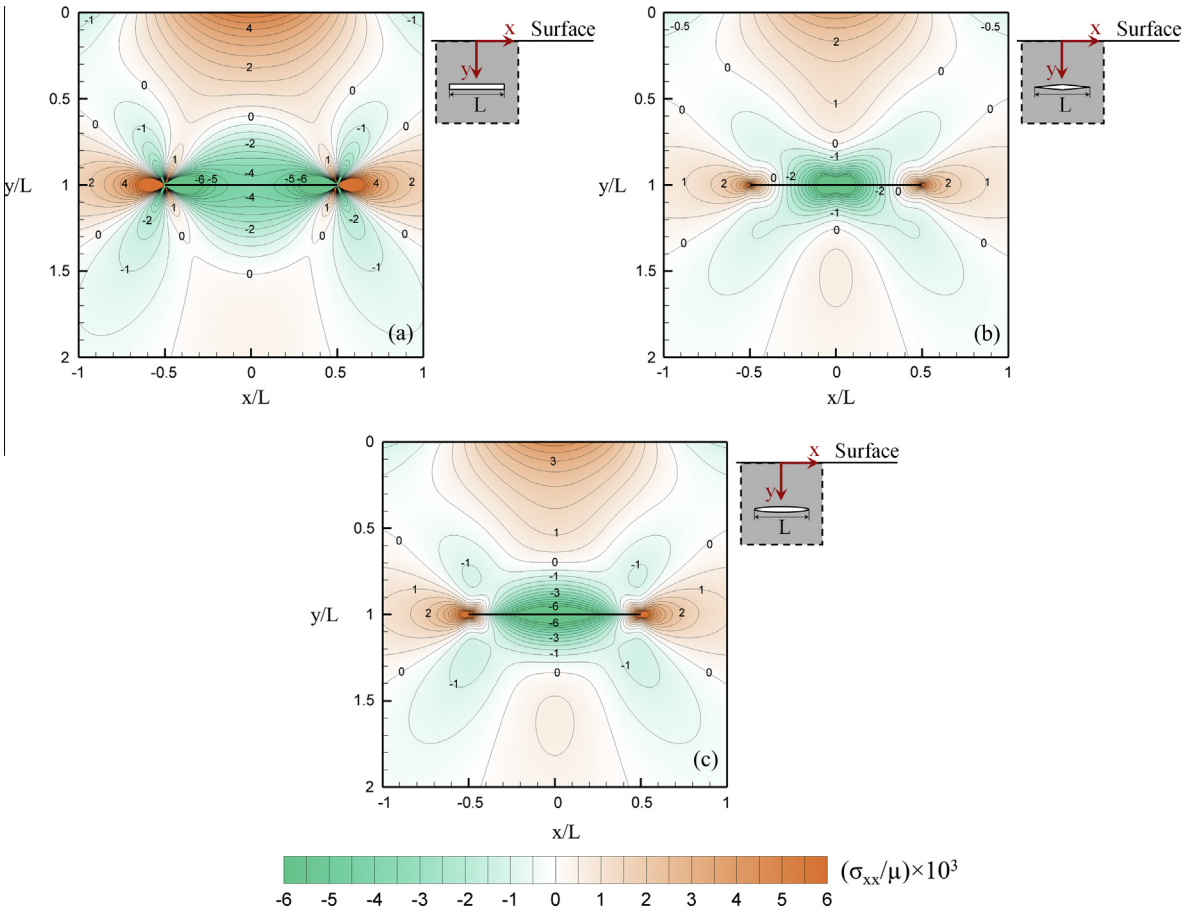

Fig. 3. Contours of σ_{xx}/μ for a horizontal DD, with length $L = 1$ m, located at $y/L = 1.0$ in the half plane for (a) uniform DD, (b) linear DD, and (c) quadratic DD. The surface of the half plane is located at $y = 0$. In all three cases, the maximum value of Δu_y is 0.005 m.

in a half plane. The material properties for the half plane are $\mu = 2$ GPa and $\nu = 0.25$. The crack is 1000 m below the surface so that the Crouch and Starfield [2] solution for the constant DD in the full plane can be applied. The DD profile is assumed to be quadratic, with the maximum opening being $\Delta u_y = 0.005$ m at the crack center and zero at its left and right tips. For simplicity, the horizontal component of the DD is assumed to be zero along the crack. For this case, our exact closed-form solutions of the quadratic DD can be directly applied without requiring any discretization. To see the effect of discretization, we have also applied the constant DD solution of Crouch and Starfield [2] to discretize the quadratic DD profile. Fig. 2 compares the values of σ_{xx}/μ along a line which is 0.5 m above the crack (x' line). In this figure, the dashed, dotted and thin solid curves correspond to the results using the Crouch and Starfield solution [2] with $N = 1$, 8 and 32 constant DD elements along the whole length of the crack; the thick solid curve represents the exact closed-form solution of the quadratic DD presented in this paper. In order to accurately predict the stress field induced by a quadratic DD, 32 constant DD elements are required for a maximum relative error of 3% (Table 1). Table 1 further shows the relative error percentage of using different numbers of elements, as compared to the exact closed-form solutions of quadratic DD profile. For a maximum error less than 1%, 64 constant elements are needed, indicating more computational times as compared to the exact closed-form solution presented in this paper.

In the second example, we compare the stress fields of opening-mode DDs with uniform, linear, and quadratic relative displacement profiles, respectively. In this example, each horizontal DD line has a length of 1 m located 1 m below the surface. Along the DD line, we assume only the relative opening displacements and there is no tangential displacement discontinuity (i.e., $\Delta u_x = 0$). Fig. 3a illustrates the contours of the horizontal normal stress σ_{xx} induced by the DD where Δu_y is uniform and equals 0.005 m. Fig. 3b and c shows the contours of the stresses due to the linear and quadratic variations in Δu_y, with the maximum relative discontinuity being 0.005 m at the crack center and zero at its left and right tips. The material properties are set to $\mu = 2$ GPa and $\nu = 0.25$ in each case. The vertical normal stress σ_{yy} and shear stress σ_{xy} for these three DD profiles are shown in Figs. 4 and 5, respectively. While Figs. 3–5 each show gross similarities, including a stress singularity at the tips of the DD, they differ in detail, especially along the DD. For instance, the stress singularity at the tips is stronger for constant DD than for the linear and quadratic ones, and the sign of the near-tip stress perturbation is more heterogeneous as well. In addition, Fig. 5 demonstrates considerable difference between the shear stress σ_{xy} fields induced

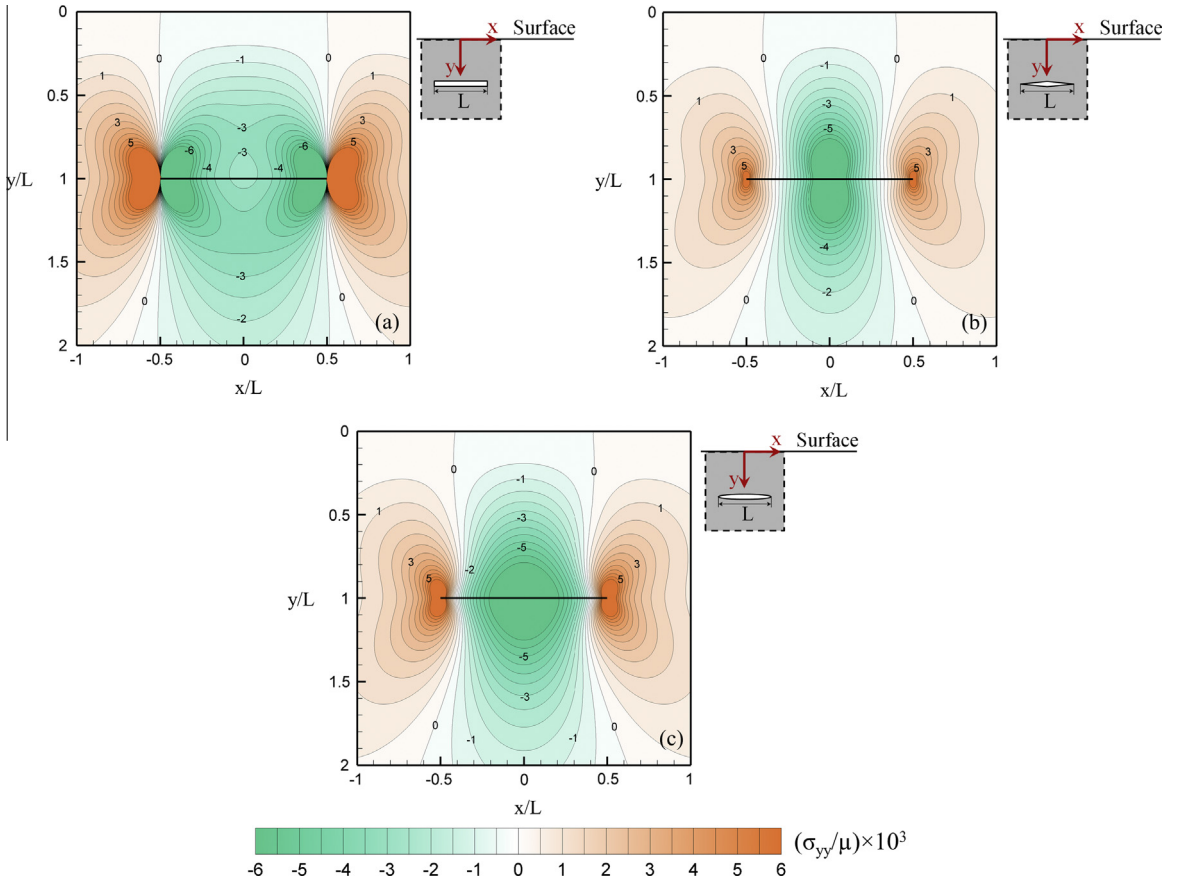

Fig. 4. Contours of σ_{yy}/μ for a horizontal DD, with length $L = 1$ m, located at $y/L = 1.0$ in the half plane for (a) uniform DD, (b) linear DD, and (c) quadratic DD. The surface of the half plane is located at $y = 0$.

by the uniform and non-uniform DDs. In particular, although the distribution of σ_{xy} is anti-symmetric on both sides of the DD, the stress gradients are less severe near the DD tips in the non-uniform cases (Fig. 5b and c) as compared to the uniform case (Fig. 5a). These figures further indicate that, except for the tips of the DD, at which discrepancies cannot be resolved due to singularity, the peak stress magnitudes due to the uniform DD are about twice the linear one, with those due to the quadratic one in between. This mirrors the relative difference between the average values of Δu_y in the three cases. Moreover, the effect of the traction-free surface located at $y = 0$ on the stress distributions can also be observed in these figures. While there are stress concentrations near the traction-free surface for the case of the normalized stress σ_{xx} (Fig. 3), the fields for the normalized stresses σ_{yy} and σ_{xy} approach zero near the free surface (Figs. 4 and 5), which partially verifies the correctness of the present formulations.

In the third example, the maximum shear stress field is calculated around an inclined normal fault represented by a shearing DD with either a uniform, linear, or quadratic relative tangential displacements. The opening component is zero along the line in each case. The normal stress perpendicular to and the shear stress parallel to the fault line are also calculated since these components control the conditions favoring slip ahead of the fault tip. The fault is a buried normal fault of length L [26] in the half plane. The lower tip is fixed at $y = 1000$ m ($y/L = 1.34$) and its upper tip is located at $y = 300$ m ($y/L = 0.4$) below the traction-free surface. The fault dips 70° and projects to intersect the surface at the origin. The average dip slip is assumed to be 0.06 m and the material parameters are $\mu = 2$ GPa and $\nu = 0.25$. We consider three cases: (a) uniform dip slip along the fault; (b) dip slip that varies linearly from a maximum at the midpoint of the fault to zero at both the upper and lower tips; and (c) dip slip of a quadratic nature, with its maximum at midpoint of the fault and slip tapering to zero at both the upper and lower tips. Again, zero normal DD is prescribed along the fault walls, i.e., the walls are required to remain in contact and neither open nor interpenetrate. The contours of the maximum shear stress around the fault for these three cases are shown in Fig. 6. In the uniform case, the stresses are strongly concentrated at the DD tip and diminish sharply towards its center (Fig. 6a). This is a result of the constant displacement discontinuity Δu terminating abruptly at the fault tips. In the case where the slip varies linearly from a peak value to zero at the model fault tips (Fig. 6b), the maximum shear stress is singular at the tip, but not as strongly singular as where the slip is constant [27]. This reflects the linear taper of the slip to zero towards the model fault tip. Additionally, an even stronger stress singularity occurs where the peak slip occurs; this reflects the discontinuity in the rate of change of the slip distribution there [27]. If the point of peak slip is close to the tip of a model fault, then the associated singularity shifts closer to the tip too. For the quadratic slip distribution (Fig. 6c), the

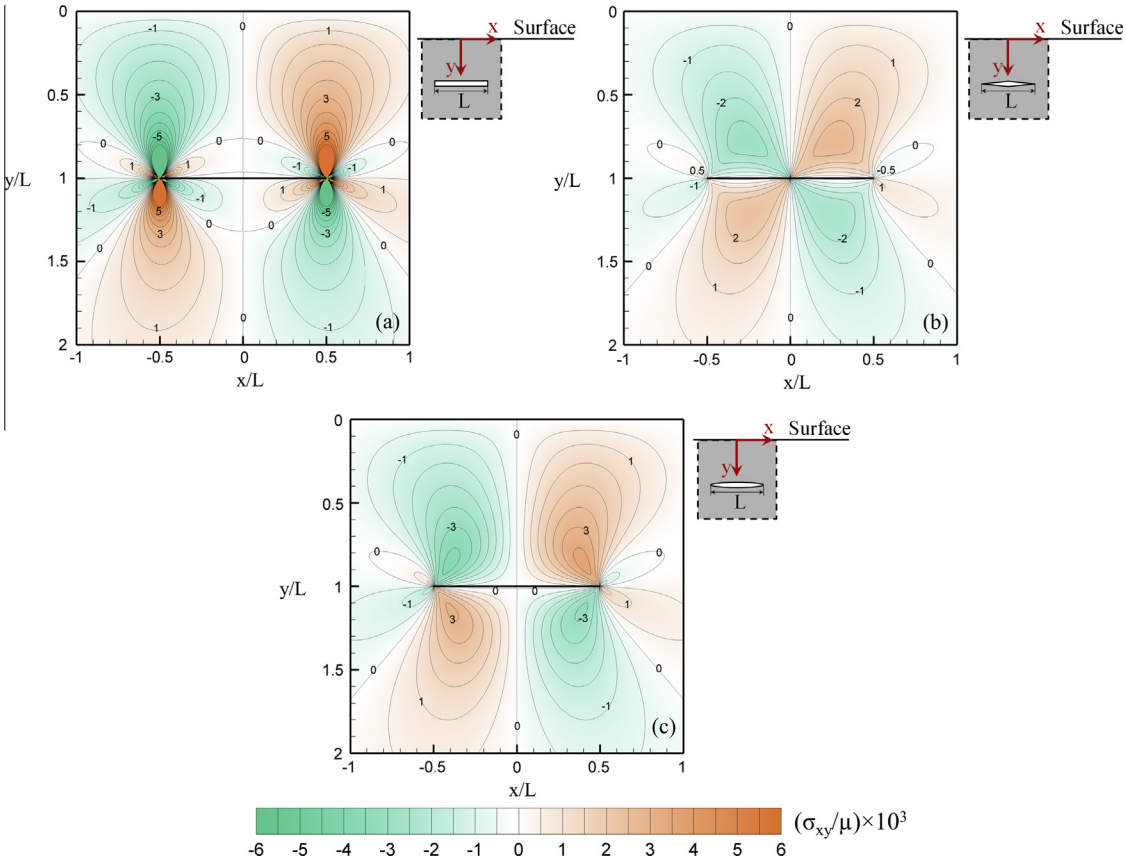

Fig. 5. Contours of σ_{xy}/μ for a horizontal DD, with length $L = 1$ m, located at $y/L = 1.0$ in the half plane for (a) uniform DD, (b) linear DD, and (c) quadratic DD. The surface of the half plane is located at $y = 0$.

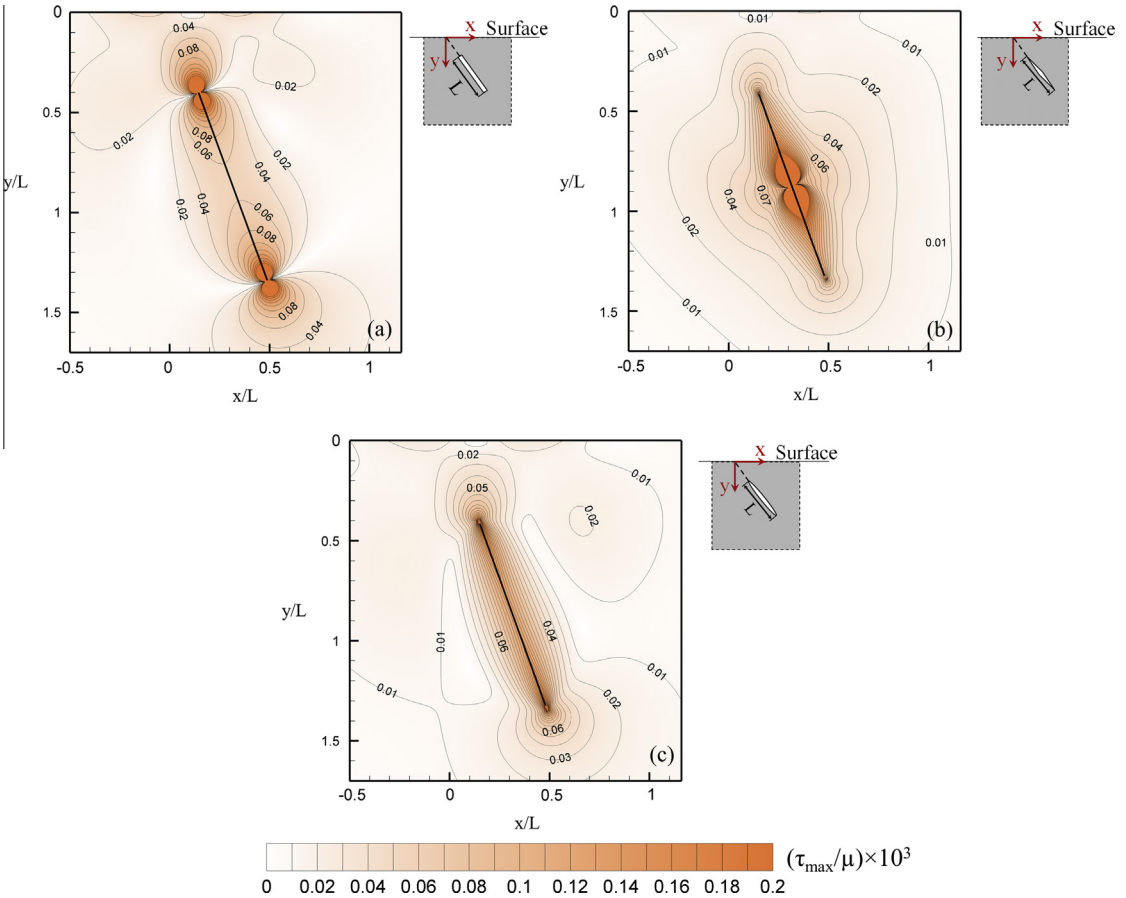

Fig. 6. Maximum shear stress induced by the dip-slip DD along an inclined normal fault with a dip of 70° (measured from the positive horizontal x-axis) in the half plane: (a) uniform DD, (b) linear DD, and (c) quadratic DD. The lower tip of the fault is at $y = 1000$ m ($y/L = 1.34$) and its upper tip is at $y = 300$ m, ($y/L = 0.4$).

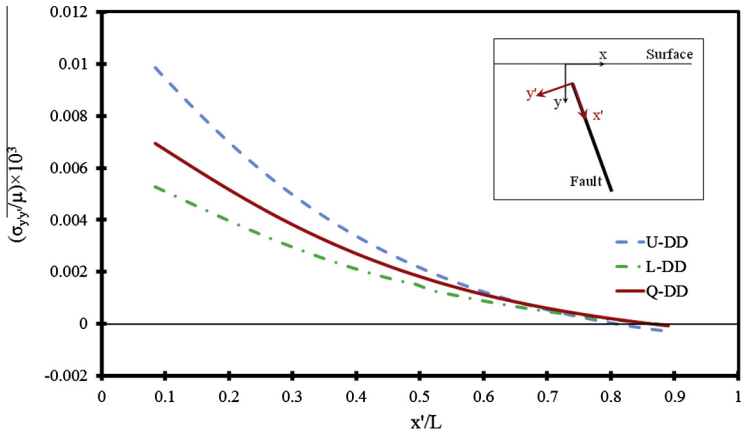

Fig. 7. Normal stress perpendicular to and along a model fault with a dip of 70° in the half plane. The lower tip of the fault is at $y = 1000$ m ($y/L = 1.34$) and its upper tip is at $y = 300$ m ($y/L = 0.4$). U-DD stands for uniform DD, L-DD for linear DD, and Q-DD for quadratic DD.

maximum shear stress distribution along the fault has an intermediate character. The stresses are more strongly concentrated near the model fault tips than where the slip varies linearly (Fig. 6b), but not as strongly concentrated as where the slip is constant (Fig. 6a). The maximum shear stress distribution along the model fault with the quadratic slip distribution (Fig. 6c) is much more uniform than where the slip is constant (Fig. 6a) or varies linearly from the slip maximum towards the model fault tips (Fig. 6b). These results imply that the secondary shear fracturing around a fault could be highly sensitive to the slip distribution. On a separate but related point, in other cases where both the slip distribution and its rate of

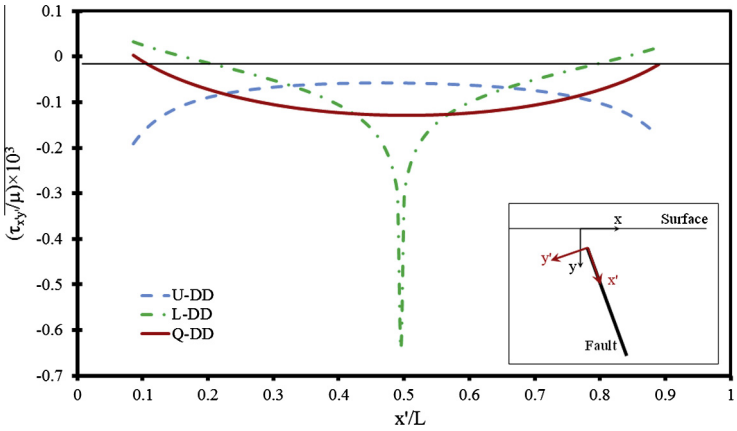

Fig. 8. Shear stress parallel to and along a model fault with a dip of 70° in the half plane. The lower tip of the fault is at y = 1000 m (y/L = 1.34) and its upper tip is at y = 300 m (y/L = 0.4). U-DD stands for uniform DD, L-DD for linear DD, and Q-DD for quadratic DD.

change taper to zero at the model fault tips, as in a so-called cohesive end zone [28], quadratic DD elements could be applied to model near-tip stresses more precisely than constant-slip elements would allow.

Along the fault, Figs. 7 and 8 show partial profiles for the normal stress $\sigma_{y'y'}$ perpendicular to the fault and for the shear stress $\sigma_{y'x'}$ parallel to the fault. Since the normal and shear stresses at the tips are singular, they have been excluded from the diagram. The normal and shear stresses are normalized with respect to one-thousandth the shear modulus. Fig. 7 shows that the distributions of normal stress $\sigma_{y'y'}$ along the faults are similar for all three cases but of different magnitudes. The largest absolute magnitude occurs where the slip is uniform and the smallest where the slip varies linearly from a peak at the fault center. The shear stresses in Fig. 8 are comparable near the middle of the fault for the uniform and quadratic slip distributions but singular for the linear case at midpoint due to discontinuity in the rate of change of the slip [27]. These variations in the slip distribution lead to non-negligible differences in the stress distributions for all stress tensor components. Therefore, the ability to accurately represent the appropriate slip distribution should help predict secondary natural or induced fractures along faults.

4. Conclusions

The exact closed-form Green's functions for a concentrated DD are utilized to derive the analytical expressions for the stress fields in the half plane induced by the quadratic relative displacement (Δu) distribution. The solution can be used to simulate a general DD by approximating the distribution with piecewise uniform, linear, or quadratic segments. Four key points emerge from our examples:

- The magnitude and shape of the stress contours near the DD depend highly on the relative displacement distribution. For an opening-mode DD, except for the tips of the DD which discrepancies cannot be resolved due to singularity, the magnitude of the stress components due to a uniform value of Δu is about twice the linear case; the magnitude of stress components due to the DD of quadratic profile lies in between.
- The distribution of the maximum shear stress around a fault modeled as a DD is different for uniform and non-uniform (linear and quadratic) slip distributions. Furthermore, along the fault, the local shear and normal stresses near the DD are also different for the three different slip distributions.
- For a model fault in a half plane, the maximum shear stress is shifted toward the surface due to the effect of the free surface.
- In cases where the slip distribution has a zero slope near the crack tips, quadratic DD elements can avoid stress singularities and hence can be used to model cohesive end zones more precisely than elements with constant displacement discontinuities.

The obtained results for an arbitrary, non-uniform distribution of relative displacement using non-linear elements may lead to more efficient numerical formulations. The methodology presented in this paper is in the exact form for a second degree, linear or uniform profile of the relative displacement. The exact closed-form solution for a non-uniform DD in the elastic isotropic half plane is unique, can be easily applied to simulate the realistic DD profile along a fracture, and can be used to calculate the stress field around a fault, hydraulic fracturing cracks, and other types of DD.

Appendix A

In order to evaluate the Γ functions in Eq. (20), we first make use of Eq. (15) so that the complex variables z and $\bar{z}$ along the straight line segment can be expressed as

$$z = x_1 + iy_1 + [(x_2 - x_1) + i(y_2 - y_1)]t$$
$$\bar{z} = x_1 - iy_1 + [(x_2 - x_1) - i(y_2 - y_1)]t \tag{A1}$$

Then the exact closed-form expressions for the Γ functions can be found as follows.

$$\Gamma_{1p,x_s} = 2L\left\{Af_1(k_1,k_2) + \overline{A}f_1(k_3,k_4)\right\}$$
$$\Gamma_{1p,y_s} = 2iL\left\{Af_1(k_1,k_2) - \overline{A}f_1(k_3,k_4)\right\} \tag{A2}$$

$$\Gamma_{1c,x_s} = 2L\{2Af_2(k_3,k_4,k_6,k_4) - (2A+B)f_1(k_6,k_4) - (2\overline{A}+\overline{B})f_1(k_5,k_2) + 2\overline{A}f_2(k_1,k_2,k_5,k_2)\}$$
$$\Gamma_{1c,y_s} = 2iL\{2Af_2(k_3,k_4,k_6,k_4) - Bf_1(k_6,k_4) + \overline{B}f_1(k_5,k_2) - 2\overline{A}f_2(k_1,k_2,k_5,k_2)\} \tag{A3}$$

$$\Gamma_{2p,x_s} = 2L\{-2Af_2(k_3,k_4,k_1,k_2) + (\overline{A}+\overline{B})f_1(k_5,k_2)\}$$
$$\Gamma_{2p,y_s} = 2iL\{-2Af_2(k_3,k_4,k_1,k_2) + (\overline{A}-\overline{B})f_1(k_5,k_2)\} \tag{A4}$$

$$\begin{aligned}\Gamma_{2c,x_s} = 2L\Big\{&(A+B)f_1(k_1,k_2) - 6\overline{A}f_3(k_8,k_9,k_{10},k_5,k_2) + (6\overline{A}+2\overline{B})f_2(k_7,k_4,k_5,k_2) + 6\overline{A}f_3(k_{13},k_{14},k_{15},k_5,k_2)\\ &-2\overline{A}f_2(k_{11},2k_2,k_5,k_2) - (4\overline{A}+2\overline{B})f_2(k_{12},k_2,k_5,k_2)\Big\}\\ \Gamma_{2c,y_s} = 2iL\Big\{&(B-A)f_1(k_1,k_2) + 6\overline{A}f_3(k_8,k_9,k_{10},k_5,k_2) - 2(\overline{A}+\overline{B})f_2(k_7,k_4,k_5,k_2) - 6\overline{A}f_3(k_{13},k_{14},k_{15},k_5,k_2)\\ &+2\overline{A}f_2(k_{11},2k_2,k_5,k_2) + 2\overline{B}f_2(k_{12},k_2,k_5,k_2)\Big\}\end{aligned} \tag{A5}$$

where functions f_1, f_2 and f_3 can be expressed as follows.

$$f_1(p,q) = \int_0^1 \frac{\alpha t^2 + \beta t + \gamma}{(p+qt)^2}dt = \alpha\left\{\frac{(2p+q)}{q^2(p+q)} + \frac{2p}{q^3}\ln\left(\frac{p}{p+q}\right)\right\} - \beta\left\{\frac{1}{q(p+q)} + \frac{1}{q^2}\ln\left(\frac{p}{p+q}\right)\right\} + \frac{\gamma}{p(p+q)} \tag{A6}$$

$$\begin{aligned}f_2(r,s,p,q) &= \int_0^1 \frac{(r+st)(\alpha t^2+\beta t+\gamma)}{(p+qt)^3}dt\\ &= \alpha\left\{\frac{-rq(2p+3q)+s(6p^2+9pq+2q^2)}{2q^3(p+q)^2} + \frac{2(3sp-rq)}{2q^4}\ln\left(\frac{p}{p+q}\right)\right\}\\ &\quad+\beta\left\{\frac{rq^2-sp(2p+3q)}{2pq^2(p+q)^2} + \frac{s}{q^3}\ln\left(\frac{p+q}{p}\right)\right\} + \frac{\gamma(2rp+sp+rq)}{2p^2(p+q)^2}\end{aligned} \tag{A7}$$

$$\begin{aligned}f_3(r,s,w,p,q) &= \int_0^1 \frac{(r+st+wt^2)(\alpha t^2+\beta t+\gamma)}{(p+qt)^4}dt\\ &= \alpha\left\{\frac{r}{3p(p+q)^3} - \frac{s}{q^3(p+q)} - \frac{s(3p+5q)}{6q^2(p+q)^3} + \frac{4p^3w}{q^4(p+q)^3} + \frac{w(30p^2+22pq+3q^2)}{3q^3(p+q)^3} + \frac{(sq-4pw)}{q^5}\ln\left(\frac{p+q}{p}\right)\right\}\\ &\quad+\beta\left\{\frac{2sp+r(3p+q)}{6p^2(p+q)^3} - \frac{qw(6p^2+15pq+11q^2)}{6q^4(p+q)^3} + \frac{w}{q^4}\ln\left(\frac{p+q}{p}\right)\right\} + \gamma\left\{\frac{r(3p^2+3pq+q^2)}{3p^3(p+q)^3} + \frac{s(3p+q)+2pw}{6p^2(p+q)^3}\right\}\end{aligned} \tag{A8}$$

with

$$\alpha = (a_x + a_y); \quad \beta = (b_x + b_y); \quad \gamma = (c_x + c_y) \tag{A9}$$

and k_1–k_{15} being the complex variables defined as follows.

$$\begin{aligned}&k_1 = x_1 + iy_1 - z_s; && k_2 = (x_2 - x_1) + i(y_2 - y_1);\\ &k_3 = x_1 - iy_1 - \bar{z}_s; && k_4 = (x_2 - x_1) - i(y_2 - y_1);\\ &k_5 = x_1 + iy_1 - \bar{z}_s; && k_6 = x_1 - iy_1 - z_s;\\ &k_7 = x_1 - iy_1; && k_8 = k_1k_7;\\ &k_9 = k_1k_4 + k_2k_7; && k_{10} = k_2k_4;\\ &k_{11} = 2x_1 + 2iy_1 - z_s; && k_{12} = x_1 + iy_1;\\ &k_{13} = k_1k_{12}; && k_{14} = k_{12}k_2 + k_2k_1;\\ &k_{15} = k_2^2\end{aligned} \tag{A10}$$

References

[1] Crouch S. Solution of plane elasticity problems by the displacement discontinuity method. I. Infinite body solution. Int J Numer Meth Engng 1976;10:301–43.
[2] Crouch S, Starfield A. Boundary element methods in solid mechanics. London: Allen and Unwin; 1983.
[3] Shou K, Crouch S. A higher order displacement discontinuity method for analysis of crack problems. Int J Rock Mech Min Sci Geomech 1995;32(1):49–55.
[4] Fares N, Li VC. An indirect boundary element method for 2-D finite/infinite regions with multiple displacement discontinuities. Engng Fract Mech 1987;26:127–41.
[5] Pan E, Amadei B. Fracture mechanics analysis of cracked 2-D anisotropic media with a new formulation of the boundary element method. Int J Fract 1996;77:161–74.
[6] Pan E. A general boundary element analysis of 2-D linear elastic fracture mechanics. Int J Fract 1997;88:41–59.
[7] Pan E, Yuan F. Boundary element analysis of three-dimensional cracks in anisotropic solids. Int J Numer Meth Engng 2000;48:211–37.
[8] Azhdari A, Obata M, Nemat-Nasser S. Alternative solution methods for crack problems in plane anisotropic elasticity, with examples. Int J Solids Struct 2000;37:6433–78.
[9] Hossaini Nasab H, Marji MF. A semi-infinite higher-order displacement discontinuity method and its application to the quasistatic analysis of radial cracks produced by blasting. Mech Mater Struct 2007;2(3):439–57.
[10] Ma G, An X, Zhang H, Li L. Modeling complex crack problems using the numerical manifold method. Int J Fract 2009;156:21–35.
[11] Zhang H, Li L, An X, Ma G. Numerical analysis of 2-D crack propagation problems using the numerical manifold method. Engng Anal Boundary Elem 2010;34:41–50.
[12] Kübbeler M, Roth I, Krupp U, Fritzen CP, Christ HJ. Simulation of stage I-crack growth using a hybrid boundary element technique. Engng Fract Mech 2011;78:462–8.
[13] Gordeliy E, Piccinin R, Napier JA, Detournay E. Axisymmetric benchmark solutions in fracture mechanics. Engng Fract Mech 2013;102:348–57.
[14] d'Alessio M, Martel SJ. Development of strike slip faults from dikes, Sequoia National Park, California. J Struct Geol 2005;27:35–49.
[15] Maerten L, Willemse EJ, Pollard DD, Rawnsley K. Slip distributions on intersecting normal faults. J Struct Geol 1999;21:259–72.
[16] Maerten L, Gillespie P, Pollard DD. Effects of local stress perturbation on secondary fault development. J Struct Geol 2002;24:145–53.
[17] Meng C, Maerten F, Pollard DD. Modeling mixed-mode fracture propagation in isotropic elastic three dimensional solid. Int J Fract 2013;179(1–2):45–57.
[18] Martel SJ. Modeling elastic stresses in long ridges with the displacement discontinuity method. Pure Appl Geophys 2000;157:1039–57.
[19] Muller J, Martel SJ. Numerical models of translational landslide rupture surface growth. Pure Appl Geophys 2000;157:1009–38.
[20] Martel SJ. Mechanics of landslide initiation as a shear fracture phenomenon. Mar Geol 2004;203:319–39.
[21] Soliva R, Maerten F, Petit JP, Auzias V. Field evidences for the role of static friction on fracture orientation in extensional relays along strike-slip faults: comparison with photoelasticity and 3-D numerical modeling. J Struct Geol 2010;32(11):1721–31.
[22] Pan E. Dislocation in an infinite poroelastic medium. Acta Mech 1991;87(1–2):105–15.
[23] Timoshenko S, Goodier JN. Theory of elasticity. 3rd ed. New York: Mc Graw-Hill Book Company; 1953.
[24] Muskhelishvili N. Some basic problems of the mathematical theory of elasticity: fundamental equations, plane theory of elasticity, torsion and bending. 3rd ed. Leiden: Noordhoff International Publishing; 1953.
[25] Maerten F, Maerten L, Cooke M. Solving 3D boundary element problems using constrained iterative approach. Comput Geosci 2010;14(4):551–64.
[26] Martel SJ, Langley JS. Propagation of normal faults to the surface in basalt, Koae fault system, Hawaii. J Struct Geol 2006;28:2123–43.
[27] Martel SJ, Shacat C. Mechanics and interpretations of fault slip. In: Earthquakes: Radiated Energy and the Physics of Faulting; 2006. p. 207–15.
[28] Martel SJ. Effects of cohesive zones on small faults and implications for secondary fracturing and fault trace geometry. J Struct Geol 1997;19(6):835–47.